

Running of the top quark mass at NNLO in QCD

Matteo M. Defranichis^a, Jan Kieseler^a, Katerina Lipka^b, Javier Mazzitelli^c

^a*CERN, EP Department, Geneva, Switzerland*

^b*University of Wuppertal and Deutsches Elektronen-Synchrotron, Hamburg, Germany*

^c*Max Planck Institute for Physics, Munich, Germany*

Abstract

The running of the top quark mass (m_t) is probed at the next-to-next-to-leading order (NNLO) in quantum chromodynamics (QCD) for the first time. The result is obtained by comparing calculations in the modified minimal subtraction ($\overline{\text{MS}}$) renormalisation scheme to a differential measurement of the top quark-antiquark ($t\bar{t}$) production cross section at $\sqrt{s} = 13$ TeV. The scale dependence of m_t is extracted as a function of the invariant mass of the $t\bar{t}$ system, up to an energy scale of about 0.5 TeV. The observed running is found to be in good agreement with the three-loop solution of the QCD renormalisation group equations.

1. Introduction

In the modified minimal subtraction ($\overline{\text{MS}}$) renormalisation scheme, the parameters of the quantum chromodynamics (QCD) lagrangian, i.e. the strong coupling constant α_s and the masses of the quarks, depend on the energy scale at which they are evaluated. This effect, often referred to as “running”, is described by the renormalisation group equations (RGEs) of QCD, which can be solved using perturbation theory. The running of the quark masses has been calculated up to order α_s^5 [1, 2]. Measurements of the running of quark masses are not only a fundamental proof of QCD as a renormalisable theory, but also an indirect probe of physics beyond the standard model. In fact, the QCD RGE would be modified e.g. in the context of supersymmetric theories [3] or in models implying dynamic mass generation [4].

Experimentally, the running of the charm quark mass was investigated using deep inelastic scattering data at the DESY HERA [5], while the running of the bottom quark mass has been demonstrated using results from the CERN LEP, SLAC SLC, DESY HERA, and CERN LHC [6, 7], up to the

scale of the Higgs boson mass. The running of the top quark mass has been investigated for the first time by the CMS Collaboration at the CERN LHC [8]. The running was extracted using a differential measurement of the $t\bar{t}$ production cross section at $\sqrt{s} = 13$ TeV and QCD calculations at next-to-leading order (NLO) in the $\overline{\text{MS}}$ scheme [9] implemented in the MCFM program [10, 11].

In this work, the CMS measurement is used to probe the running of the top quark mass at next-to-next-to-leading order (NNLO) in QCD for the first time. This is achieved using NNLO differential calculations in the $\overline{\text{MS}}$ scheme [12] implemented in the MATRIX framework [13] that were not available at the time of the CMS measurement. This analysis also benefits from a significantly improved fit procedure, which allows for a consistent treatment of the numerical uncertainty in the theoretical predictions. This becomes necessary due to the increased numerical uncertainties in the NNLO calculations, which are limited by computing time and resources. Furthermore, variations of the renormalisation and factorisation scales are now fully taken into account.

Similar to the work of Ref. [8], the present analysis is performed solely in the framework of QCD. Electroweak corrections, which may play a relevant role in the relation between the top quark pole and $\overline{\text{MS}}$ masses [14], are not taken into account in this context as they are not implemented in any calculation in the $\overline{\text{MS}}$ scheme which includes NNLO QCD effects.

2. Theoretical setup and experimental inputs

In the CMS analysis of Ref. [8], the dependence of the running top quark mass $m_t(\mu_m)$ is investigated as a function of the scale $\mu_m = m_{t\bar{t}}$, where $m_{t\bar{t}}$ is the invariant mass of the $t\bar{t}$ system. In the calculation, the renormalisation (μ_r), factorisation (μ_f), and top quark mass (μ_m) scales are all set to the value of m_t . In each bin of $m_{t\bar{t}}$ independently, the value of $m_t(m_t)$ is extracted by performing a χ^2 fit of the theoretical calculation to the measured cross section. The extracted values of $m_t(m_t)$ are then converted to the corresponding values of $m_t(\mu_k)$ using one-loop solutions of the RGEs, where μ_k is the representative energy scale of bin k in $m_{t\bar{t}}$, corresponding to the average $m_{t\bar{t}}$ value in that bin. The bin boundaries for $m_{t\bar{t}}$ and the corresponding values of μ_k are reported in Table 1.

Following the approach suggested in Ref. [12], the CMS analysis was repeated by setting the scale μ_m to $\mu_k/2$, independently in each bin of $m_{t\bar{t}}$.

bin (k)	$m_{t\bar{t}}$ [GeV]	μ_k [GeV]
1	< 420	384
2	420 – 550	476
3	550 – 810	644
4	> 810	1024

Table 1: Boundaries of the $m_{t\bar{t}}$ bins and scales μ_k as defined in Ref. [8].

This choice is preferred over μ_k due to the fact that $\mu_k/2$ corresponds approximately to m_t in the vicinity of the $t\bar{t}$ production threshold, which is the value typically used in the calculation of the total cross section. Furthermore, the bin-by-bin dynamic scale choice allows the value of $m_t(\mu_k/2)$ to be determined directly. The two approaches were found to yield consistent results [15].

In this work, the approach proposed in Ref. [12] is adopted, and NNLO calculations are used for the first time for the extraction of $m_t(\mu_m)$. Unlike in Ref. [15], the μ_r , μ_f , and μ_m central scales in the calculation are all set to $\mu_k/2$, and scale uncertainties are estimated by varying μ_r and μ_f by a factor of two, avoiding cases in which $\mu_r/\mu_f = 4$ or $1/4$. The scale μ_m is not varied in this context, as it represents the independent variable with respect to which the running is extracted. The calculation is interfaced with the ABMP16_5_nnlo [16] set of parton distribution functions (PDFs), and the $t\bar{t}$ production cross section is calculated in each bin of $m_{t\bar{t}}$ for different values of $m_t(\mu_k/2)$. In the calculation, the value of α_S is set consistently with that of the PDFs. A comparison between the NLO and NNLO predictions and the CMS measurement of Ref. [8] can be found in Ref. [12]. The PDF uncertainties are estimated by performing the calculation using the complete set of PDF eigenvectors. In each bin, the PDF uncertainties are estimated with respect to a reference mass point, chosen such that the calculated cross section for that mass is close to the measured one in order to minimise any possible extrapolation bias. The relative PDF uncertainties obtained with this procedure are assumed to be independent of the value of the top quark mass. This approximation is necessary in order to keep the computing time within an acceptable range. Finally, in the case of the ABMP16_5_nnlo PDFs, the uncertainty in the value of α_S is included in the PDF variations.

The differential cross section measured in Ref. [8] is re-scaled in order to take into account the latest measurement of the total integrated luminosity by the CMS experiment [17]. This implies both a shift in the central values

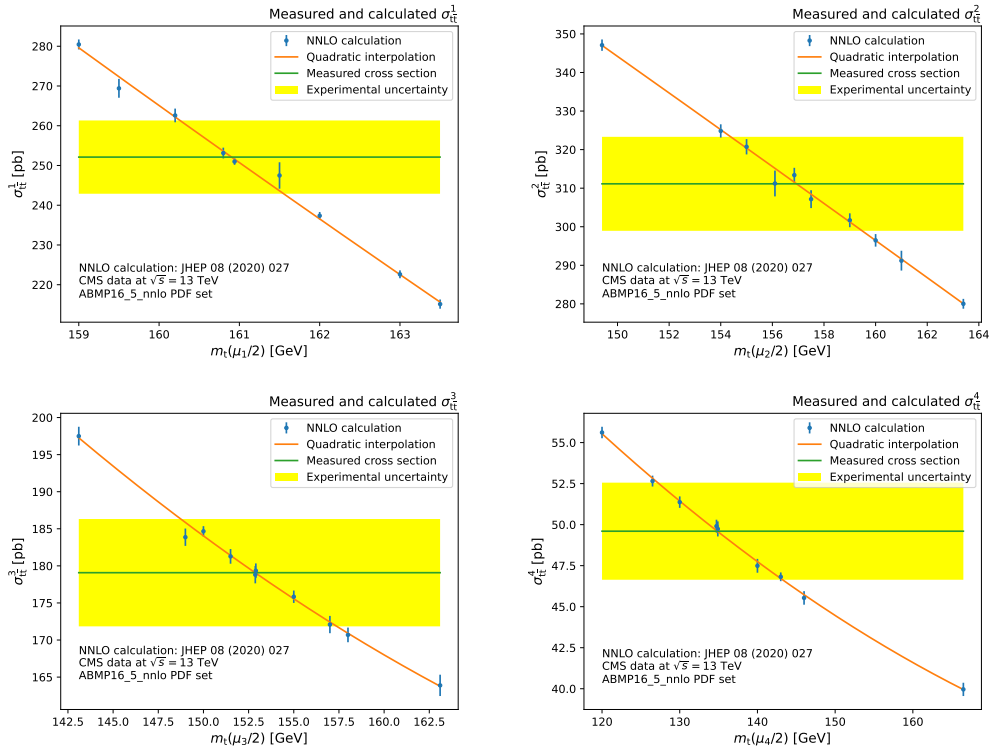


Figure 1: Calculated $t\bar{t}$ production cross section ($\sigma_{t\bar{t}}^k$) in bin k of $m_{t\bar{t}}$ as a function of $m_t(\mu_k/2)$ (points) compared to the re-scaled value of the measured cross section of Ref. [8] (horizontal lines). The vertical error bars represent the numerical uncertainty in the theoretical predictions, while the horizontal error bands correspond to the re-scaled uncertainty in the measured cross sections. The dependence of the calculated cross section on the value of $m_t(\mu_k/2)$ is parameterised assuming a quadratic dependence (line).

of the measured differential cross section and a reduction in the luminosity uncertainty from 2.5% to 1.2%. The covariance matrix between the bins is re-calculated accordingly by subtracting (adding) the covariance matrix corresponding to the old (new) luminosity uncertainty, assuming a fully correlated effect in the different bins. The obtained results are compared to the NNLO theoretical predictions as a function of $m_t(\mu_k/2)$ in Figure 1. The dependence of the calculated cross section on the values of $m_t(\mu_k/2)$ is found to be well described by a second-order polynomial.

3. The fit procedure

An improved fit procedure compared to the one of Ref. [8] is developed for this work. The values of $m_t(\mu_k/2)$ are extracted simultaneously by means of a χ^2 fit of the theoretical prediction to the measured differential cross section. The χ^2 is parameterised as a function of the values of $m_t(\mu_k/2)$ and of the nuisance parameters representing the effect of the numerical uncertainties in the NNLO calculation and the PDF uncertainties on the predicted differential cross section. This allows the numerical uncertainties and their correlations with the other parameters of the fit to be consistently taken into account, avoiding any possible bias in the determination of the running. As for the PDF uncertainties, this approach is equivalent to the ABMP16_5_nnlo prescription [16]. The χ^2 function can be written in the form:

$$\chi^2(\vec{m}, \vec{j}, \vec{\eta}) = \vec{\Delta}^T(\vec{m}, \vec{j}, \vec{\eta}) C_{\text{exp}}^{-1} \vec{\Delta}(\vec{m}, \vec{j}, \vec{\eta}) + \sum_{p=1}^{\text{nPDF}} j_p^2 + \sum_{t=1}^{\text{nPred}} \eta_t^2, \quad (1)$$

where

$$\Delta_k(m_k, \vec{j}, \vec{\eta}) = \sigma_{\text{exp}}^k - \sigma_{\text{th}}^k(m_k, \vec{j}, \vec{\eta}). \quad (2)$$

Here, \vec{m} represents the free parameters used to determine the values of $m_t(\mu_k/2)$, while \vec{j} and $\vec{\eta}$ are the nuisance parameters modelling the effect of the PDF uncertainties and numerical uncertainties in the calculated cross sections, respectively. Furthermore, σ_{exp}^k and σ_{th}^k correspond to the values of the measured and calculated cross sections in bin k of $m_{t\bar{t}}$, respectively, the latter depending on the \vec{m} , \vec{j} , and $\vec{\eta}$ parameters. The matrix C_{exp} represents the covariance between the bins of the measured differential cross section, and it includes the effect of the experimental and extrapolation uncertainties described in Ref. [8]. For asymmetric extrapolation uncertainties, the maximum between the positive-side and negative-side variations is conservatively

taken. The first term in Eq. 1 is the statistical term, while the two following ones are Gaussian penalty terms representing the prior assumptions on the nuisance parameters. In the fit, all nuisance parameters are defined such that they follow a standard normal distribution. The index p runs up to the number of PDF variations, $\text{nPDF} = 29$, while the index t runs up to the number of theoretical predictions used in the fit, nPred , which include the 38 mass points and the 29 PDF variations.

The effect of the numerical uncertainties is modelled by introducing modifiers to the calculated cross sections that depend on the corresponding nuisance parameter and the size of the numerical uncertainty. For each calculated cross section σ_{th}^t , including those obtained for the various PDF eigenvectors, the quantity $\sigma_{\text{th}}^t(\eta_t)$ is defined:

$$\sigma_{\text{th}}^t(\eta_t) = \sigma_{\text{th}}^t(1 + \eta_t \delta_{\text{num}}^t), \quad (3)$$

where δ_{num}^t is the relative numerical uncertainty in σ_{th}^t . For each nominal mass point m in bin k of $m_{\text{t}\bar{\text{t}}}$, the dependence of the calculated cross section on the PDF variations is then estimated as:

$$\sigma_{\text{th}}^{m,k}(\vec{j}, \vec{\eta}) = \sigma_{\text{th}}^{m,k}(\eta_{m,k}) \prod_{p=1}^{\text{nPDF}} \left[1 + j_p \left(\frac{\sigma_{\text{th}}^{p,k}(\eta_{p,k})}{\sigma_{\text{th}}^{m_0,k}(\eta_{m_0,k})} - 1 \right) \right], \quad (4)$$

where $\sigma_{\text{th}}^{m_0,k}$ is the nominal cross section for the reference mass point m_0 used to derive the PDF variations in bin k (see Section 2), and $\sigma_{\text{th}}^{p,k}$ is the calculated cross section corresponding to the PDF variation p for the reference mass point. In Eq. 4, all calculated cross sections are corrected for their numerical uncertainties according to Eq. 3.

The quantities $\sigma_{\text{th}}^{m,k}(\vec{j}, \vec{\eta})$ are then used to derive the dependence of the calculated cross section on $m_k = m_{\text{t}}(\mu_k/2)$. For each choice of values for \vec{j} and $\vec{\eta}$, the dependence $\sigma_{\text{th}}^k(m_k)$ is estimated by means of a quadratic interpolation, as shown in Figure 1. This way the theoretical dependence on m_k is smoothed and the impact of the numerical uncertainties mitigated. Furthermore, the correlations between the different mass points introduced by the PDF variations are fully taken into account in the interpolation procedure. These correlations arise from the fact that a single mass point is used to derive the dependence on the PDF variations.

Finally, the uncertainties related to the choice of μ_{r} and μ_{f} are estimated by repeating the fit for different scale choices. The maximum variation observed in each bin, which in all cases correspond to one of the combined

variations of μ_r and μ_f , is conservatively taken as the scale uncertainty in that bin. The correlations between the scale variations in the different bins are kept track of, and an additional covariance matrix is derived.

4. Results

In Figure 2, the extracted $m_t(\mu_k/2)$ are compared with the evolved value of $m_t(m_t)$ obtained in Ref. [18]. The value of $m_t(m_t)$ was extracted from a measurement of the inclusive $t\bar{t}$ cross section at $\sqrt{s} = 13$ TeV using NNLO predictions and the same PDF set as in this work. The numerical values of the $m_t(\mu_k/2)$ are reported in Table 2. The experimental (exp) uncertainty, corresponding to the total uncertainty in the measured differential cross section, is obtained by fixing all the \vec{j} and $\vec{\eta}$ parameters to their post-fit values. The combination between PDF and numerical uncertainties is then obtained by subtracting in quadrature the experimental component from the total uncertainty, and is denoted with ‘‘PDF+num’’. In this analysis the PDF and numerical uncertainties are strongly correlated, therefore their individual impacts are not estimated.

$\mu_k/2$ [GeV]	$m_t(\mu_k/2)$ [GeV]	exp [GeV]	PDF+num [GeV]	scale [GeV]
192	160.90	0.61	0.81	+0.13, -0.69
238	156.9	2.5	2.4	+1.4, -3.0
322	152.9	4.2	4.4	+4.4, -6.7
512	134.8	8.7	7.0	+9.0, -12.2

Table 2: Extracted values of $m_t(\mu_k/2)$ and their uncertainties. The experimental (exp) component is obtained by freezing all the nuisance parameters to their post-fit values, while the combination between PDF and numerical uncertainties (PDF+num) is obtained by subtracting in quadrature the experimental component from the total uncertainty. The scale uncertainty refers to the variations of μ_r and μ_f .

Following the strategy of Ref. [8], the running is defined with respect to the reference scale $\mu_{\text{ref}} = \mu_2/2 = 238$ GeV. The choice of the reference scale is arbitrary, and does not affect the conclusions of the analysis. The quantities $r_k = m_t(\mu_k/2)/m_t(\mu_2/2)$ are derived and compared to the RGE prediction for $m_t(\mu_m)/m_t(\mu_2/2)$. The advantage of this approach is the cancellation of the correlated components of the systematic uncertainties in the $m_t(\mu_k/2)$. Furthermore, the scale dependence of the QCD running is probed independently of the value of m_t . The RGE is solved at three loops in QCD

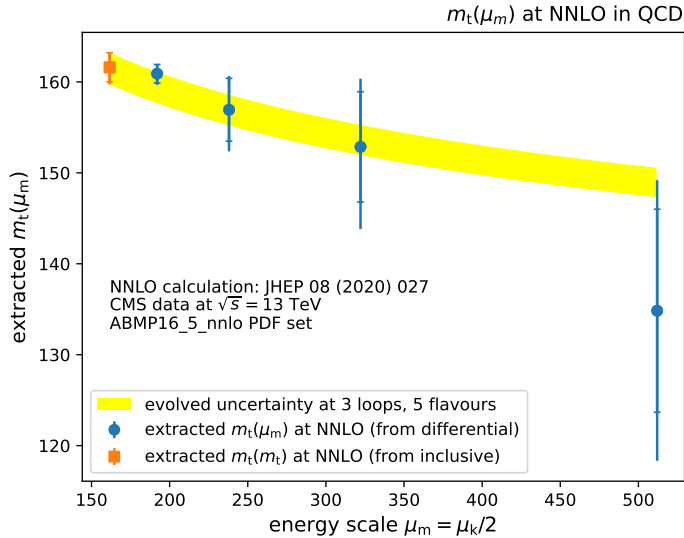


Figure 2: Extracted $m_t(\mu_k/2)$ (circles) compared to the value of $m_t(m_t)$ (squared) obtained from the inclusive $t\bar{t}$ production cross section [18]. The inner vertical bars represent the combination of experimental, PDF, and numerical uncertainties, while the outer bars also include the QCD scale uncertainties. The band represent the evolved total uncertainty in $m_t(m_t)$.

assuming 5 active flavours, consistently with the calculation of Ref. [12], using the CRUNDEC program [19]. Good agreement between the measured points and the RGE prediction is observed, as shown in Figure 3. The reduced χ^2 between the RGE and the measured r_k is obtained in the Gaussian approximation by combining the covariance matrix from the χ^2 fit to that corresponding to the scale variations. A reduced χ^2 of 0.49 is obtained, which corresponds to a p -value of 69%, reflecting the good agreement between the RGE prediction and the observed running of m_t .

5. Summary

The running of the top quark mass is studied at next-to-next-to-leading order (NNLO) in quantum chromodynamics (QCD) for the first time. The analysis makes use of NNLO QCD predictions in the $\overline{\text{MS}}$ scheme based on the MATRIX framework [13] and implemented in Ref. [12], and of a differential measurement of the top quark-antiquark ($t\bar{t}$) production cross section from

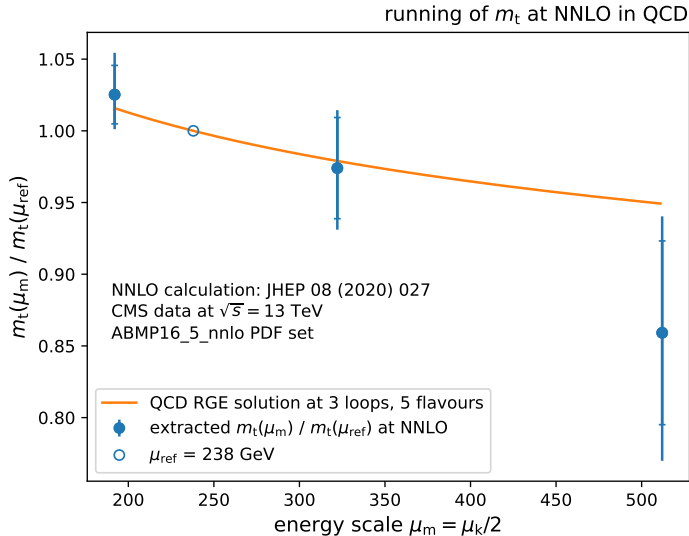


Figure 3: Extracted running of the top quark mass (full markers) normalised to the reference energy scale of 238 GeV (hollow marker), compared to the 3-loop solution of the QCD RGE assuming 5 active flavours (line). The inner vertical bars represent the combination of experimental, PDF, and numerical uncertainties, while the outer bars also include the QCD scale uncertainties.

the CMS experiment at the CERN LHC [8]. The running is extracted as a function of the invariant mass of the $t\bar{t}$ system by means of a χ^2 fit of the theoretical predictions to the measured cross section. The analysis benefits from a significantly improved fit procedure, developed for the purpose of this work, which consistently takes into account the numerical uncertainties in the calculation and their correlations with the other parameters of the fit. The extracted running is found to be in good agreement with the solution of the QCD renormalisation group equations, within experimental and theoretical uncertainties.

Acknowledgements

We are sincerely grateful to Massimiliano Grazzini, Stefano Catani, and Sven-Olaf Moch for fruitful discussions on the theoretical aspects of this work. JM is grateful to Stefano Catani, Simone Devoto, Massimiliano Grazzini, and Stefan Kallweit for their contribution in the development of the results of Ref. [12], and for many fruitful discussions.

References

- [1] P. A. Baikov, K. G. Chetyrkin, J. H. Kühn, Quark Mass and Field Anomalous Dimensions to $\mathcal{O}(\alpha_s^5)$, JHEP 10 (2014) 076. [arXiv:1402.6611](#), [doi:10.1007/JHEP10\(2014\)076](#).
- [2] T. Luthe, A. Maier, P. Marquard, Y. Schröder, Five-loop quark mass and field anomalous dimensions for a general gauge group, JHEP 01 (2017) 081. [arXiv:1612.05512](#), [doi:10.1007/JHEP01\(2017\)081](#).
- [3] L. Mihaila, Precision calculations in supersymmetric theories, Adv. High Energy Phys. 2013 (2013) 607807. [arXiv:1310.6178](#), [doi:10.1155/2013/607807](#).
- [4] N. D. Christensen, R. Shrock, Implications of dynamical generation of standard-model fermion masses, Phys. Rev. Lett. 94 (2005) 241801. [arXiv:hep-ph/0501294](#), [doi:10.1103/PhysRevLett.94.241801](#).
- [5] A. Gizhko, et al., Running of the charm-quark mass from HERA deep-inelastic scattering data, Phys. Lett. B 775 (2017) 233. [arXiv:1705.08863](#), [doi:10.1016/j.physletb.2017.11.002](#).
- [6] O. Behnke, A. Geiser, M. Lisovskyi, Charm, beauty and top at HERA, Prog. Part. Nucl. Phys. 84 (2015) 1. [arXiv:1506.07519](#), [doi:10.1016/j.ppnp.2015.06.002](#).
- [7] J. Aparisi, et al., m_b at m_H : The running bottom quark mass and the Higgs boson, Phys. Rev. Lett. 128 (2022) 122001. [arXiv:2110.10202](#), [doi:10.1103/PhysRevLett.128.122001](#).
- [8] CMS Collaboration, Running of the top quark mass from proton-proton collisions at $\sqrt{s} = 13$ TeV, Phys. Lett. B 803 (2020) 135263. [arXiv:1909.09193](#), [doi:10.1016/j.physletb.2020.135263](#).
- [9] M. Dowling, S.-O. Moch, Differential distributions for top-quark hadro-production with a running mass, Eur. Phys. J. C 74 (2014) 3167. [arXiv:1305.6422](#), [doi:10.1140/epjc/s10052-014-3167-x](#).
- [10] J. M. Campbell, R. K. Ellis, MCFM for the Tevatron and the LHC, Nucl. Phys. B Proc. Suppl. 205-206 (2010) 10–15. [arXiv:1007.3492](#), [doi:10.1016/j.nuclphysbps.2010.08.011](#).

- [11] J. M. Campbell, R. K. Ellis, Top-quark processes at NLO in production and decay, *J. Phys. G* 42 (2015) 015005. [arXiv:1204.1513](#), [doi:10.1088/0954-3899/42/1/015005](#).
- [12] S. Catani, S. Devoto, M. Grazzini, S. Kallweit, J. Mazzitelli, Top-quark pair hadroproduction at NNLO: differential predictions with the $\overline{\text{MS}}$ mass, *JHEP* 08 (2020) 027. [arXiv:2005.00557](#), [doi:10.1007/JHEP08\(2020\)027](#).
- [13] M. Grazzini, S. Kallweit, M. Wiesemann, Fully differential NNLO computations with MATRIX, *Eur. Phys. J. C* 78 (2018) 537. [arXiv:1711.06631](#), [doi:10.1140/epjc/s10052-018-5771-7](#).
- [14] A. L. Kataev, V. S. Molokoedov, Notes on interplay of the QCD and EW perturbative corrections to the pole-running top-quark mass ratio, *JETP Letters* (2022). [arXiv:2201.12073](#), [doi:10.1134/S0021364022600902](#).
- [15] M. M. Defranchis, Top quark mass and cross sections in ATLAS and CMS, in: *55th Rencontres de Moriond on QCD and High Energy Interactions*, 2021, pp. 143–148. [arXiv:2105.05776](#).
- [16] S. Alekhin, J. Blümlein, S. Moch, R. Placakyte, Parton distribution functions, α_s , and heavy-quark masses for LHC Run II, *Phys. Rev. D* 96 (2017) 014011. [arXiv:1701.05838](#), [doi:10.1103/PhysRevD.96.014011](#).
- [17] CMS Collaboration, Precision luminosity measurement in proton-proton collisions at $\sqrt{s} = 13$ TeV in 2015 and 2016 at CMS, *Eur. Phys. J. C* 81 (2021) 800. [arXiv:2104.01927](#), [doi:10.1140/epjc/s10052-021-09538-2](#).
- [18] CMS Collaboration, Measurement of the $t\bar{t}$ production cross section, the top quark mass, and the strong coupling constant using dilepton events in pp collisions at $\sqrt{s} = 13$ TeV, *Eur. Phys. J. C* 79 (2019) 368. [arXiv:1812.10505](#), [doi:10.1140/epjc/s10052-019-6863-8](#).
- [19] B. Schmidt, M. Steinhauser, CRUNDEC: a C++ package for running and decoupling of the strong coupling and quark masses, *Comput. Phys. Commun.* 183 (2012) 1845. [arXiv:1201.6149](#), [doi:10.1016/j.cpc.2012.03.023](#).